

UCSF

UC San Francisco Previously Published Works

Title

Distal Hydrogen-bonding Interactions in Ligand Sensing and Signaling by Mycobacterium tuberculosis DosS*

Permalink

<https://escholarship.org/uc/item/9rm4m3kh>

Journal

Journal of Biological Chemistry, 291(31)

ISSN

0021-9258

Authors

Basudhar, Debashree
Madrona, Yarrow
Yukl, Erik T
[et al.](#)

Publication Date

2016-07-01

DOI

10.1074/jbc.m116.724815

Peer reviewed

Distal Hydrogen-bonding Interactions in Ligand Sensing and Signaling by *Mycobacterium tuberculosis* DosS*

Received for publication, March 1, 2016, and in revised form, April 28, 2016 Published, JBC Papers in Press, May 27, 2016, DOI 10.1074/jbc.M116.724815

Debashree Basudhar[‡], Yarrow Madrona[‡], Erik T. Yukl^{§1}, Santhosh Sivaramakrishnan[‡], Clinton R. Nishida[‡], Pierre Moënne-Loccoz[§], and Paul R. Ortiz de Montellano^{‡2}

From the [‡]Department of Pharmaceutical Chemistry, University of California at San Francisco, San Francisco, California 94158-2517 and the [§]Division of Environmental and Biomolecular Systems, Institute of Environmental Health, Oregon Health Science University, Portland, Oregon 97239-3098

Mycobacterium tuberculosis DosS is critical for the induction of *M. tuberculosis* dormancy genes in response to nitric oxide (NO), carbon monoxide (CO), or hypoxia. These environmental stimuli, which are sensed by the DosS heme group, result in autophosphorylation of a DosS His residue, followed by phosphotransfer to an Asp residue of the response regulator DosR. To clarify the mechanism of gaseous ligand recognition and signaling, we investigated the hydrogen-bonding interactions of the iron-bound CO and NO ligands by site-directed mutagenesis of Glu-87 and His-89. Autophosphorylation assays and molecular dynamics simulations suggest that Glu-87 has an important role in ligand recognition, whereas His-89 is essential for signal transduction to the kinase domain, a process for which Arg-204 is important. Mutation of Glu-87 to Ala or Gly rendered the protein constitutively active as a kinase, but with lower autophosphorylation activity than the wild-type in the Fe(II) and the Fe(II)-CO states, whereas the E87D mutant had little kinase activity except for the Fe(II)-NO complex. The H89R mutant exhibited attenuated autophosphorylation activity, although the H89A and R204A mutants were inactive as kinases, emphasizing the importance of these residues in communication to the kinase core. Resonance Raman spectroscopy of the wild-type and H89A mutant indicates the mutation does not alter the heme coordination number, spin state, or porphyrin deformation state, but it suggests that interdomain interactions are disrupted by the mutation. Overall, these results confirm the importance of the distal hydrogen-bonding network in ligand recognition and communication to the kinase domain and reveal the sensitivity of the system to subtle differences in the binding of gaseous ligands.

Tuberculosis, an airborne disease caused by *Mycobacterium tuberculosis*, is believed to have infected nearly 1 out of 3 people worldwide (1). Like any infection, tuberculosis leads to a host immune response resulting in recruitment of lymphocytes and

macrophages (2). This process is associated with high levels of NO and CO produced by inducible nitric-oxide synthase and heme oxygenase-1 (HO-1), respectively, as part of the defense mechanism of macrophages (3–5). The ability of *M. tuberculosis* to successfully survive within the host for years in a clinically undetectable dormant state known as non-replicating persistence (NRP)³, in which it is resistant to most of the currently available treatments, makes it of paramount importance to elucidate this defense strategy (6). The mechanism of NRP is not fully understood; however, hypoxia (7, 8), high CO and NO levels (5, 9), nutrient deprivation (10), and the pH of the microenvironment (11) are among the factors leading to NRP. It has been shown that NRP can initiate changes in energy metabolism and cellular signaling pathways that lead to *M. tuberculosis* growth arrest. Decreased cellular activity is believed to be the main reason for the long term treatment protocols required to eradicate the bacteria. Moreover, in recent years, multiple drug-resistant and extremely drug-resistant strains of *M. tuberculosis* have emerged (12). Thus, the primary goal of new drug discovery is to design novel molecules to overcome drug resistance and to shorten the period of treatment.

Dormancy survival proteins DosS, also known as DevS, and DosT play an important role in this context. DosS and DosT are histidine kinase proteins with 61% sequence identity that, after intramolecular phosphorylation of one of their His residues, transfer the phosphate group to Asp-45 of the response regulator protein DosR. This induces the onset of 48 dormancy-related genes (13). DosT is constitutively expressed both in the presence and absence of O₂, although DosS is induced by hypoxia as well as by CO and NO, two key players in the host defense mechanism. DosS is also induced by ascorbate and menaquinone under aerobic conditions (14). DosS and DosT have been shown to play an important role in the transition from the replicating state to NRP (15). Recently, Gautam *et al.* (16) showed that DosS has a critical role in survival of *M. tuberculosis* in C3HeB/FeJ mice, whereas deletion of DosR and DosT gave rise to a growth curve comparable with that of wild-type *M. tuberculosis*. Kumar *et al.* (17) demonstrated the importance of DosS by showing that induction of *M. tuberculosis* dormancy by CO depended primarily on sensing by DosS. These studies suggest that inhibition of DosS would block *M. tuberculosis*

* This work was supported by National Institutes of Health Grants AI074824 (to P. R. O. M.) and GM74785 (P. M.-L.). The authors declare that they have no conflicts of interest with the contents of this article. The content is solely the responsibility of the authors and does not necessarily represent the official views of the National Institutes of Health.

¹ Present address: Dept. of Chemistry and Biochemistry, New Mexico State University, Las Cruces, NM 88003-8001.

² To whom correspondence should be addressed: University of California at San Francisco, 600 16th St., San Francisco, CA 94158-2517. Tel.: 415-476-2903; Fax: 415-502-4728; E-mail: ortiz@cgl.ucsf.edu.

³ The abbreviations used are: NRP, non-replicating persistence; RMSF, root mean squared fluctuation.

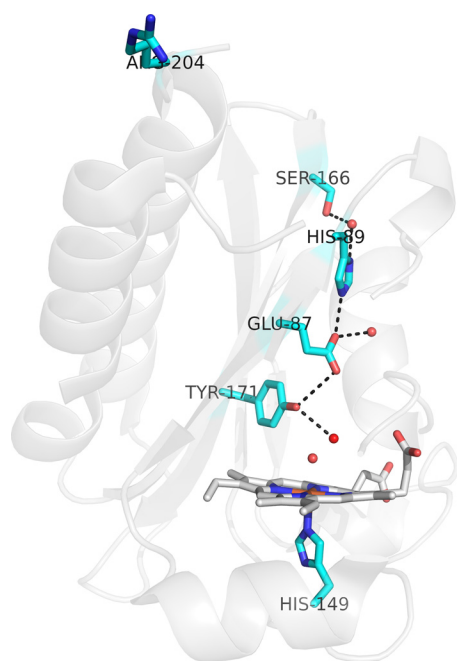


FIGURE 1. Crystal structure of the ferric DosS GAF-A(63–210) domain (Protein Data Bank code 2W3E) showing the proximal histidine ligand and the distal hydrogen-bonding network. A hydrogen bond between Arg-204 and His-89 is not evident in the crystal structure but is observed in the molecular dynamics simulations.

from entering into the NRP state and hence that DosS is a potential target for drug design.

DosS contains two adjacent GAF domains, GAF-A and GAF-B. GAF-A has a heme prosthetic group, although the function of the GAF-B domain, which has no heme, remains unclear. DosS also has a kinase core with an ATP binding domain and a histidine phosphate-accepting domain that upon autophosphorylation initiates the signaling cascade (18). The crystal structure of the DosS GAF-A domain identifies His-149 as the proximal iron ligand and Tyr-171 as a highly conserved residue close to the heme (Fig. 1) (19). UV-visible and resonance Raman spectroscopy clearly demonstrate that DosS binds reversibly to O₂, CO, and NO (20). In the presence of O₂, DosS exhibits little autophosphorylation activity, whereas deoxy DosS and its ferrous CO and NO complexes show strong, time-dependent catalytic activity. The Y171F mutant loses its ability to discriminate between O₂, CO, and NO and has little kinase activity with all three ligands; however, the deoxy Y171F mutant retains an activity similar to that of wild-type deoxy DosS (21). The importance of Tyr-171 is supported by the crystal structure, which shows a hydrogen-bonding network extending from a water molecule coordinated to ferric heme center through the side chains of Tyr-171, Glu-87, and His-89 (19). Reduction of the heme iron causes dissociation of the heme-bound water molecule and alteration of the hydrogen-bonding network with repositioning of Glu-87 and His-89 (19).

To understand the ability of DosS to differentially sense diatomic gases, we investigated the role of the distal hydrogen-bonding network by site-directed mutagenesis of Glu-87 and His-89 combined with autophosphorylation activity assays, UV-visible and resonance Raman spectroscopy, and molecular

dynamics simulations. The effect of Arg-204 was also examined based on the molecular dynamics results.

Materials and Methods

Site-directed Mutagenesis and Cloning of the DosS Distal Mutants—The full-length *doss* gene containing a C-terminal His₆ tag and engineered NdeI and BamHI restriction sites, previously constructed by amplification from *M. tuberculosis* H37Rv genomic DNA into a pET23a+ vector, was used as the template for mutagenesis (20). Site-directed mutagenesis was carried out using the QuikChange Lightning site-directed mutagenesis kit (Agilent, Santa Clara, CA, catalogue no. 210518) according to the prescribed protocol. The plasmid was then digested using NdeI and BamHI restriction enzymes (New England Biolabs, Ipswich, MA) and subcloned into a fresh pET23a+ vector. The resulting plasmid was verified using DNA sequencing. The E87A, E87D, E87G, H89A, H89R, and R204A mutants were prepared by this method.

Expression of the Full-length and Mutant DosS Proteins—Full-length DosS and its mutants were expressed and purified following the previously reported procedure with only minor modifications (20). The full-length *doss* construct in a pET23a+ vector was transformed into pT-GroE-transformed BL21(DE3) gold competent cells. A single colony was picked from an LB/AMP/chloramphenicol plate and grown overnight in LB medium containing ampicillin (100 μg/ml) and chloramphenicol (50 μg/ml). Approximately 20 ml of the overnight culture was transferred to 1.5 liters of LB culture medium containing ampicillin (100 μg/ml) and chloramphenicol (50 μg/ml). The cells were grown to A₆₀₀ = 1.5 at 37 °C and 230 rpm, after which 1 mM 5-aminolevulinic acid was added. Protein expression was induced at 18 °C with isopropyl 1-thio-β-D-galactopyranoside at a final concentration of 0.2 mM. The culture was allowed to grow for a further 48 h, after which the cells were harvested by centrifugation at 5000 rpm at 4 °C for 20 min.

Protein Purification—The cells were lysed in 50 mM phosphate buffer (pH 7.5), containing 250 mM NaCl, 10% glycerol, 1% Triton X-100, 0.5 mg/ml lysozyme, 0.1 mM phenylmethylsulfonyl fluoride (PMSF), and one complete EDTA-free protease inhibitor mixture tablet (Sigma and Roche Applied Science catalogue no.11873580001). The cell suspension was stirred at room temperature for 30 min, after which the cell membranes were disrupted by repeated sonication cycles at 50% (8 × 45-s cycles with 2 min cooling in-between) using a Branson model 450 Sonifier (VWR Scientific, Visalia, CA). The resulting mixture was centrifuged at 20,000 rpm for 60 min at 4 °C.

The supernatant was applied to a 5-ml HisTrap nickel affinity column (GE Healthcare) followed by washing with 20 column volumes of 50 mM phosphate buffer (pH 7.5), containing 10% glycerol and 300 mM NaCl. The column was further washed with the same buffer containing 10, 20, 40, and 80 mM imidazole (5 column volumes each) before the protein was eluted with a 200 mM final concentration of imidazole. The protein was dialyzed overnight in a dialysis buffer (50 mM Tris-HCl (pH 7.5), containing 5% glycerol and 1 mM EDTA). The protein was then purified using a DEAE-Sepharose column using a gradient elution from 0 to 400 mM NaCl in 50 mM Tris buffer (pH 7.5), containing 5% glycerol and 1 mM EDTA. The fractions contain-

Hydrogen-bonding Network in *Mycobacterium tuberculosis* DosS

ing the protein were pooled, concentrated using an Amicon filter (30-kDa MWCO), aliquoted, and stored at -80°C for future use.

UV-visible Spectroscopy—The UV-visible spectra of wild-type DosS and its mutants were obtained on an Agilent Hewlett-Packard 8453 diode-array spectrophotometer. The spectrophotometer was blanked with Tris-HCl buffer (pH 7.5) pretreated with Chelex 100 resin containing 50 mM KCl and 5 mM MgCl_2 . The ferric protein was purged with argon and transferred to the glovebox. A few microliters of 100 mM sodium dithionite were then added to reduce the protein. The reduced protein was passed through a Sephadex PD-10 column (GE Healthcare) equilibrated with Tris-HCl buffer (pH 7.5) pretreated with Chelex 100 resin containing 50 mM KCl and 5 mM MgCl_2 to remove excess sodium dithionite. Reduced wild-type DosS and its mutants were exposed to diethylammonium (Z)-1-(*N,N*-diethylamino)diazen-1-ium-1,2-diolate (100 mM stock prepared in 10 mM of NaOH) or a saturated solution of CO or O_2 in Tris-HCl buffer (pH 7.5) containing 50 mM KCl and 5 mM MgCl_2 . The value $\epsilon_{430} = 130 \text{ mM}^{-1} \text{ cm}^{-1}$ was used for the ferrous protein, based on the value of $166 \text{ mM}^{-1} \text{ cm}^{-1}$ for the ferric protein and a scaling factor that reflects the difference in absorbance of the ferric and ferrous protein (20, 21). The formation of the Fe(II)-NO, Fe(II)-CO, and Fe(II)- O_2 complexes was measured at a λ_{max} of 419, 422, and 414 nm, respectively, although the oxygen complex was often not observed and was replaced by a maximum at 421 nm due to autoxidation to the ferric state.

Resonance Raman Spectroscopy—Typical protein concentrations for the resonance Raman experiments were $\sim 100 \mu\text{M}$ for the Fe(III) and deoxy Fe(II) forms and $\sim 300 \mu\text{M}$ for the O_2 , CO, and NO complexes. Ultrafree-0.5 ultrafiltration devices (Millipore) were used to concentrate the protein in 20 mM HEPES buffer (pH 7.5) with 150 mM NaCl. Reduction to the ferrous state was achieved by adding a few microliter aliquots of concentrated sodium dithionite solution (50 mM) to argon-purged samples. ^{12}C O (Airgas) and ^{13}C O (99% ^{13}C ; ICON Stable Isotopes) adducts were obtained by injecting CO through a septum-sealed capillary containing argon-purged, reduced protein ($\sim 20 \mu\text{l}$). NO (Airgas), $^{15}\text{N}^{18}\text{O}$ (98% ^{15}N , 95% ^{18}O ; Aldrich), O_2 (Airgas), and $^{18}\text{O}_2$ (99% ^{18}O ; ICON Stable Isotopes) adducts were obtained after removal of excess dithionite from the reduced samples by ultrafiltration by injecting the gases in septum-sealed capillaries. These procedures were performed in a glove box with a controlled atmosphere of less than 1 ppm O_2 (Omni-Lab System; Vacuum Atmospheres Co.). All samples were monitored by UV-visible spectroscopy directly in the capillary using a Cary 50 spectrometer (Varian). Resonance Raman spectra were obtained on a custom McPherson 2061/207 spectrograph (0.67 m with variable gratings) equipped with a Princeton Instruments liquid N_2 -cooled CCD detector (LN-1100PB). The excitation wavelengths were the 413- or 442-nm emission of a krypton laser (Innova 302, Coherent) and an He/Cd laser (Liconix 4240NB), respectively. Spectra were collected in a 90° scattering geometry on samples at room temperature. Supernotch or long-wave pass filters (Supernotch filters, Kaiser Optics, and RazorEdge Raman filters, Semrock) were used to attenuate the Rayleigh scattering. Frequencies were cal-

ibrated relative to indene and CCl_4 and are accurate to $\pm 1 \text{ cm}^{-1}$. CCl_4 was also used to check the polarization conditions. The integrity of the resonance Raman samples was confirmed by direct monitoring of their UV-visible spectra in the Raman capillaries before and after laser illumination.

Autophosphorylation Assays—An aliquot of wild-type or mutant DosS in 50 mM Tris-HCl buffer (pH 7.5) was placed inside the glovebox along with sodium dithionite and ATP (Sigma). The proteins were then reduced with excess dithionite (~ 10 – 15 mM) followed by its removal using a Sephadex column (PD-10, GE Healthcare) equilibrated with Tris-HCl buffer (pH 7.5) pretreated with Chelex 100 resin containing 50 mM KCl and 5 mM MgCl_2 . The UV-visible spectrum of the resulting protein was measured inside the glovebox to verify the concentration of the Fe(II) protein at the appropriate λ_{max} using $\epsilon = 130 \text{ mM}^{-1} \text{ cm}^{-1}$. A 40- μl aliquot of the reduced protein was placed into each of four different septum-sealed microcentrifuge tubes. The reactions were initiated by addition of 5 μl of assay buffer, 100 μM final concentration of diethylammonium (Z)-1-(*N,N*-diethylamino)diazen-1-ium-1,2-diolate, or 5 μl of a saturated solution of CO or O_2 . Each tube containing 45 μl of reaction mixture was taken out of the glovebox along with 20 μl of a 2 mM solution of cold ATP (Sigma). A 5- μl aliquot of [γ - ^{32}P]ATP (PerkinElmer Life Sciences, 6000 Ci/mmol, 10 mCi/ml) was added to 20 μl of 2 mM unlabeled ATP solution (Sigma). The phosphorylation reaction was initiated by addition of 5 μl of the above ATP solution to each microcentrifuge tube. All the reaction mixtures (50 μl) contained a final concentration of 5 μM DosS protein, 100 mM Tris-HCl (pH 7.5), 50 mM KCl, 5 mM MgCl_2 , and a final ATP concentration of 200 μM (10 μCi). Aliquots (10 μl) removed at 3-, 6-, 9-, and 12-min time points were mixed with 5 μl of stop buffer (SDS loading buffer containing 10% 2-mercaptoethanol). These samples were loaded onto a 15% polyacrylamide gel (Criterion, Bio-Rad) and run at 150 V for 1 h. The gel was then vacuum-dried at 80°C for 1 h and subsequently exposed in a PhosphorImager cassette (Molecular Dynamics) for 20 h. The levels of phosphorylated protein were imaged on a Storm 840 PhosphorImager (Amersham Biosciences) and quantified using ImageJ (National Institutes of Health). Phosphorylation of the wild-type Fe(II)-CO-bound protein stopped at the 20-min time point was used as a control for quantification purposes. The loading consistency was confirmed using Coomassie staining.

Molecular Dynamics Studies—Starting x-ray crystal coordinates for the wild-type, E87A, E87G mutants of the DosS-GAF-A domain were taken from Protein Data Bank codes 2W3E, 2Y79, and 2Y8H, respectively. The Visual Molecular Dynamics (22) 2.10 psfgen and solvate plugins were used to add hydrogen atoms and bulk solvent (8 Å cushion in the *x*, *y*, and *z* directions from the protein surface) and to generate a PSF topology file for simulation. The input force fields included the CHARMM36 (23) protein force field (top_all36_pro.rtf) for protein atoms, the accompanying water, ion force field for water (toppar_water_ions.str), and heme force field for the DosS heme moiety (toppar_all36_prot_heme.str). Active site crystallographic waters within 4 Å of the heme iron and active site residues 171, 87, and 89 were also included. The iron to nitrogen bond between the heme iron and the coordinating

histidine was added by referencing the PHEM patch available in the heme force field parameters. Charge on the system was neutralized with sodium ions using the Visual Molecular Dynamics Autoionize plugin.

All simulations were carried out on the shared UCSF cluster using the NAMD 2.10 molecular dynamics software package (24). Simulations were carried out at a constant temperature and pressure with rigid bonds set to "ALL" and periodic boundary conditions. System charges were calculated using the Particle Mesh Ewald method with PMEGridSpacing = 1.0. Additional force field parameters included cutoff distance = 12 Å, switchdist = 10 Å, and pairlistdist = 14 Å. Initial equilibrations of surrounding water were carried out by holding protein atoms fixed for 4000 steps for 1-fs per step. Subsequently, energy minimization was carried out for 2 ns using 1-fs time steps. Simulations for later analysis were then carried out for not less than 40 ns using 2-fs time steps.

Results

UV-visible Spectral Analysis of Wild-type DosS and Its Mutants—The Fe(III)-DosS native protein exhibited a Soret absorbance at 407 nm and Q-bands at 500 and 630 nm in the visible region, in accordance with the previously reported spectral values for this protein (25). Reduction of the protein to the Fe(II) state with dithionite caused a red shift of the Soret maximum to 430 nm, with a Q-band at 560 nm. The Fe(II)-CO form of DosS had a strong and sharp absorbance maximum at 422 nm with Q-bands at 540 and 568 nm. The NO-bound protein displayed a strong absorbance at 419 nm with two broad bands at 545 and 576 nm. Exposure of wild-type Fe(II) DosS to O₂ resulted in rapid formation of the Fe(III) state, as reported by others (26). However, on pretreating the buffer with Chelex 100 to remove metal ions, the Fe(II)-O₂ complex was formed in the presence of O₂ with a Soret maximum at 421 nm (27).

The E87D, E87G, E87A, H89A, H89R, and R204A mutants had UV-visible spectra very similar to that of the wild-type protein in the Fe(II), Fe(II)-CO, and Fe(II)-NO states (Fig. 2). However, the Fe(II)-O₂ spectra of the H89R, H89A, and R204A mutants exhibited Soret absorbance bands at 407, 409, and 408 nm, respectively (Fig. 2, A, B, and F), comparable with the bands in their respective Fe(III) spectrum, indicating autoxidation of the oxy-heme center to the ferric state. However, the H89A spectra for the Fe(II)-O₂ complex in the resonance Raman studies exhibited the formation of a reasonably stable complex, emphasizing the sensitivity of the complex to small differences in the solution conditions. Furthermore, the E87G mutant had a Soret band at 425 nm (Fig. 2D). The similarity of the Fe(II)-O₂ Soret band of the E87G mutant to that of the wild-type protein suggested formation of a reasonably stable oxyferrous species. The E87D and E87A mutants had a λ_{max} of 412 and 414 nm, respectively (Fig. 2, C and E), slightly higher than that of the ferric protein (λ_{max} 407 nm), which is likely due to the presence of a mixture of the Fe(II)-O₂ and Fe(III) forms. The heme centers of the E87D and E87A mutants thus exhibit an increased sensitivity to oxygen-dependent autoxidation relative to the wild-type and E87G mutant.

The close similarity of the UV-visible spectra of all the mutants in the Fe(II), Fe(II)-CO, and Fe(II)-NO states (Fig. 2)

suggests that the distal mutations do not significantly alter the heme binding pocket in DosS. The UV-visible data clearly suggest that some mutations increased the sensitivity of the heme-oxy complex to autoxidation, but precise autoxidation rates were not measured.

Resonance Raman of the H89A Mutant—To better evaluate possible changes at the heme center that might contribute to signaling, we compared by resonance Raman spectroscopy the wild-type and the H89A variant, which has the most differentiated catalytic behavior (see below). High frequency resonance Raman spectra of the ferric and ferrous H89A variant protein obtained with a 413-nm excitation are virtually superimposable to that of wild-type DosS (Fig. 3A), supporting conserved porphyrin geometries, iron spin states, and coordination numbers in both the oxidized and reduced proteins. Specifically, the ferric proteins exhibit a 6-coordinate high spin/low spin mixture assigned to the presence of an aqua/hydroxy distal ligand, although the ferrous proteins are pure 5-coordinate high spin species bound to the proximal histidine, His-149. Low frequency resonance Raman spectra of the reduced proteins obtained with a 442-nm excitation further support the lack of rearrangement of the heme binding pocket in the H89A variant, which exhibits an intense band at 214 cm⁻¹ assigned to an Fe-His stretching vibration, $\nu(\text{Fe-N}_{\text{His}})$, and peripheral propionate and vinyl C-C-C deformation modes at 364 and 408 cm⁻¹, as observed previously in wild-type DosS (Fig. 3B).

The resonance Raman spectra of the O₂ complexes also show remarkable conservation between the wild-type and H89A proteins. In both wild-type and variant proteins, the Fe-O₂ stretching mode, $\nu(\text{Fe-O}_2)$, is observed at 564 cm⁻¹ and shifts to 541 cm⁻¹ with ¹⁸O₂ (Fig. 4A). Previous studies have shown that the $\nu(\text{Fe-O}_2)$ mode is conserved in full-length DosS and in the truncated GAF-A domain (28). However, different conformers were observed when the CO and NO adducts were compared (28). Specifically, resonance Raman spectra of the wild-type GAF-A domain identified two CO complex conformers as follows: one with a $\nu(\text{CO})$ at 1936 cm⁻¹ that represents a carbonyl ligand hydrogen-bonded to Tyr-171, and one with a $\nu(\text{CO})$ at 1971 cm⁻¹ that represents a carbonyl ligand free of hydrogen bond interactions. Only the latter conformer was observed in the full-length wild-type protein and in the construct that included both the GAF-A and GAF-B domains (28). These differences between full-length and GAF-A proteins were interpreted in terms of restricted conformational flexibility of the heme distal pocket through interdomain interactions between the GAF-A and GAF-B domains (28). Remarkably, the resonance Raman spectra of the CO complex of full-length H89A shows the same two conformers previously seen only in the truncated GAF-A wild-type construct (Fig. 4B), suggesting that the H89A mutation might disrupt interdomain interactions in DosS and the control it provides on carbonyl conformers at the heme distal pocket.

The resonance Raman characterization of the nitrosyl complexes is less discriminative than for the CO complexes because the $\nu(\text{NO})$ frequencies approach those of strong porphyrin vibrations and lead to Fermi coupling between $\nu(\text{NO})$ and porphyrin vibrations. Despite these spectral perturbations, ¹⁴N¹⁶O–¹⁵N¹⁸O difference spectra of full-length H89A more

Hydrogen-bonding Network in *Mycobacterium tuberculosis* DosS

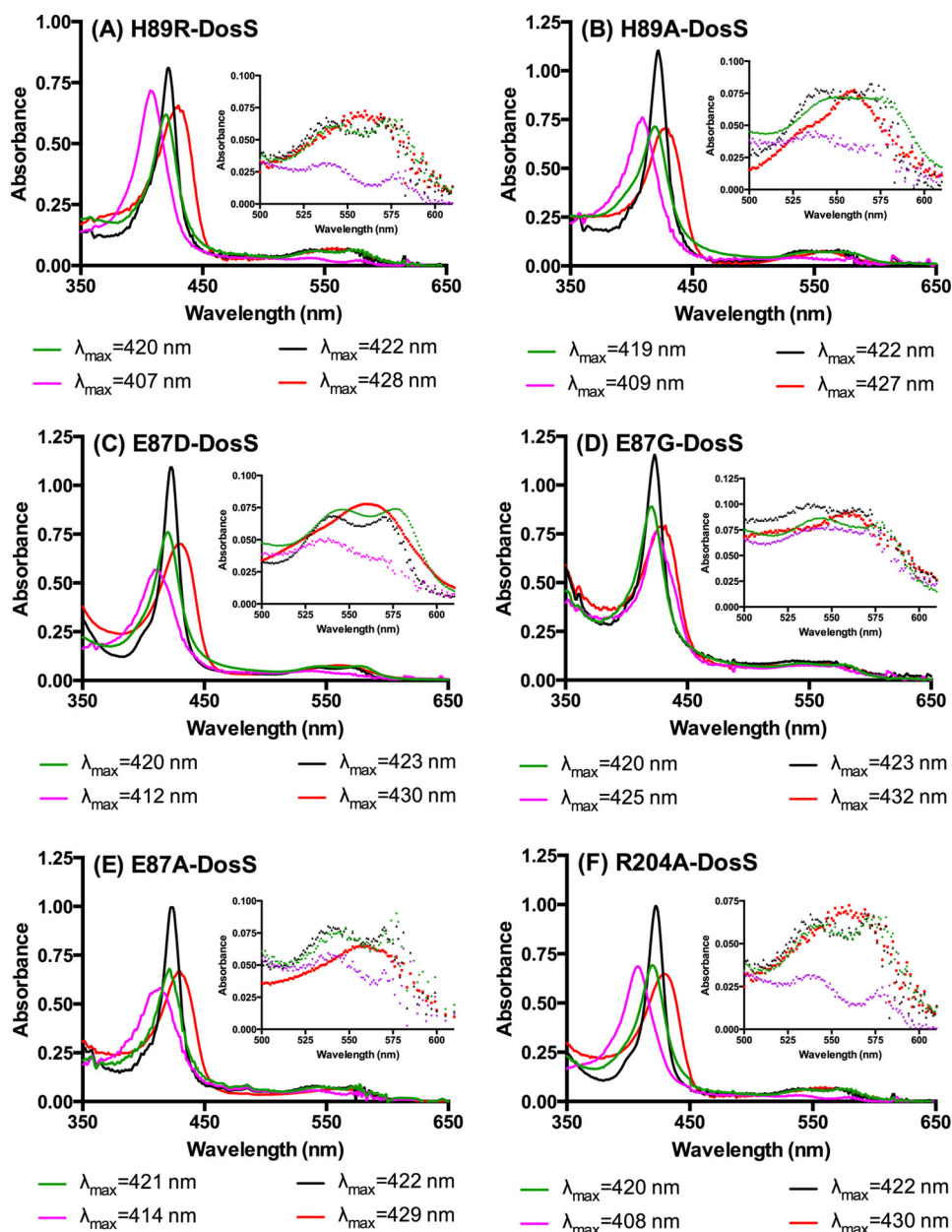


FIGURE 2. UV-visible spectrophotometric characterization of the H89R (A), H89A (B), E87D (C), E87G (D), E87A (E), and R204A (F) mutants in the Fe(II) unligated state (red) and coordinated with CO (black), NO (green), and after exposure to O₂ (magenta). This latter condition in most cases resulted in complete or nearly complete autoxidation to the Fe(III) state.

closely match those obtained with the truncated GAF-A protein than with wild-type DosS (Fig. 4C). As described previously (28), positive Raman bands at 1638 cm⁻¹ are assigned to $\nu(\text{NO})$ modes from nitrosyl conformers free of hydrogen bond interactions, although distinctive negative bands near 1530 cm⁻¹ are assigned to $\nu(^{15}\text{N}^{18}\text{O})$ modes from a nitrosyl engaged in hydrogen bond interaction(s) within the heme distal pocket.

Kinase Activity of Wild-type DosS and Its Mutants—The activities of the proteins were measured using an autophosphorylation assay in which the proteins, both in the deoxy and ligand bound states, were incubated with [γ -³²P]ATP for varying times to measure the extent and time dependence of DosS phosphorylation. Previous studies have shown that the Fe(II)-deoxy, Fe(II)-CO, and Fe(II)-NO DosS complexes have signifi-

cant activity (25, 26, 29). The relative activities for each form of the protein were measured with respect to the corresponding activity of the Fe(II)-CO form of wild-type DosS at the 20-min time point determined simultaneously, as described under “Experimental Procedures.” More importantly, the wild-type and the mutant proteins remained ligand-bound during the entire time of the assay, as judged by UV-visible spectroscopy conducted under identical conditions. Furthermore, adding a saturated solution of an appropriate gas to the deoxy protein or purging the sealed Eppendorf tubes containing the deoxy protein with the gas led to the same results.

Wild-type DosS, as expected, was active in the Fe(II)-deoxy, Fe(II)-NO, and Fe(II)-CO forms and had little activity in the O₂-bound form; the general trend in the activity of the wild-

type protein was consistent with earlier reports (25, 26, 29). As we were interested in looking at the initial rate of the reaction, the autophosphorylation reactions were monitored at 3, 6, 9, and 12 min. As shown in Fig. 5A, the activities of the protein in all forms showed a time-dependent increase. Mutations of His-89 to arginine (H89R) and of Glu-87 to aspartic acid (E87D) were expected to preserve the active site hydrogen-bonding network, whereas the H89A and E87G mutants should disrupt this network (Fig. 1).

Distal Histidine Mutants (H89R and H89A)—The H89R mutant on binding of NO or CO was about 50% less active than

the corresponding wild-type complexes (Table 1), although the deoxy and Fe(II)-O₂ forms had little activity (Fig. 5B). The H89A mutant, in which the hydrogen-bonding interactions should be completely disrupted, did not show significant autophosphorylation activity for any form of the protein (Fig. 5C and Table 1), demonstrating the importance of this network for protein activity.

Earlier, the important role of Tyr-171 in ligand recognition was demonstrated by the finding that in the Y171F mutant only the Fe(II)-deoxy protein exhibited autophosphorylation activity; all the other forms had little kinase activity (25). The present results argue that disrupting the hydrogen bonding of His-89 to Tyr-171 via Glu-87 interferes with communication of the signal to the kinase domain, as even the deoxy form without a ligand has little activity.

Distal Glutamate Mutants (E87G, E87D, and E87A)—Mutation of Glu-87 to Gly had a minimal effect on autophosphorylation of the Fe(II) deoxy and Fe(II)-NO states (Fig. 5E and Table 1). However, this mutation diminished the activity of the Fe(II)-CO complex. Interestingly, the Fe(II)-O₂ protein had much higher activity than the wild type, which had little activity. Although the E87D mutant was expected to retain its activity on ligand binding, as it can participate in hydrogen-bonding interactions, it was in fact active only with NO, although the Fe(II) and Fe(II)-CO forms had negligible activity, and the mixture of Fe(II)-O₂ and Fe(III) obtained after exposure to O₂ had no measurable activity (Fig. 5F and Table 1). Mutation of Glu-87 to Ala reduced the activity of the Fe(II) and Fe(II)-CO proteins by half compared with the wild type. The mixture of Fe(II)-O₂ and Fe(III) obtained on exposure to O₂ showed a

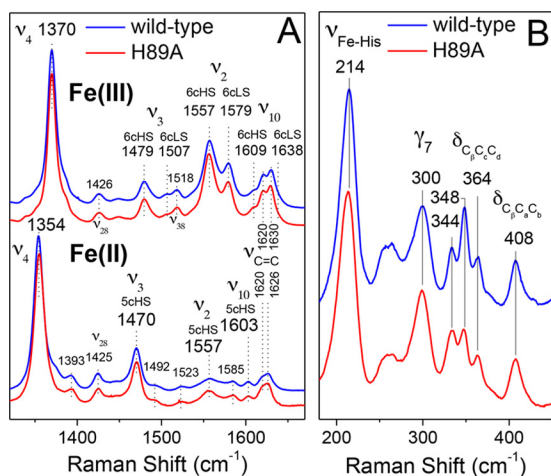


FIGURE 3. High frequency resonance Raman spectra of ferric and ferrous wild-type and H89A variant proteins obtained with a 413-nm excitation (A) and low frequency resonance Raman spectra of ferrous wild-type and H89A variant proteins obtained with a 442-nm excitation (B).

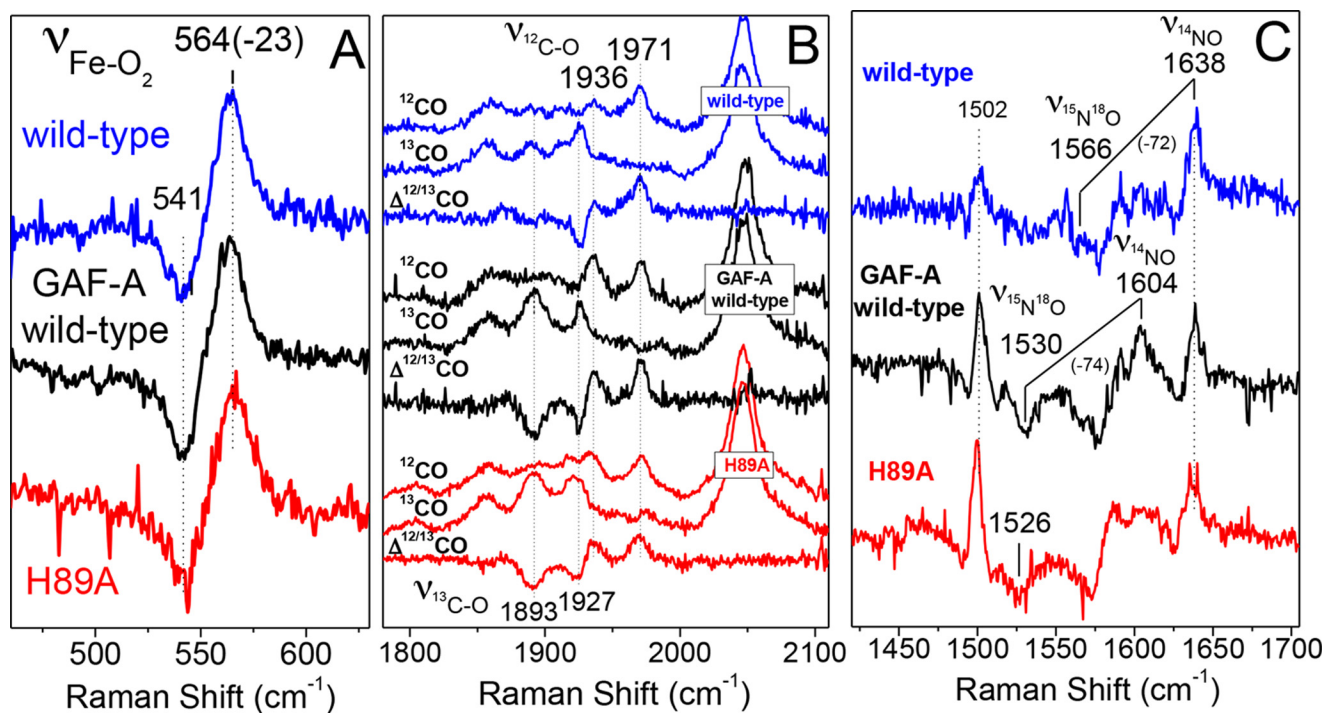


FIGURE 4. Low frequency ¹⁶O₂-¹⁸O₂ resonance Raman difference spectra of the oxy complexes of full-length wild-type (blue trace), GAF-A wild-type domain (black trace), and full-length H89A (red trace) DosS proteins (A); high frequency spectra of the carbonyl complexes formed with ¹²CO, ¹³CO, and the resulting ¹²CO-¹³CO difference spectra (B), and ¹⁴N¹⁶O-¹⁵N¹⁸O difference spectra of the nitrosyl complexes (C) of full-length wild-type (blue traces), GAF-A wild-type domain (black traces), and full-length H89A (red traces) DosS proteins. All spectra were obtained at room temperature with a 413-nm excitation.

Hydrogen-bonding Network in *Mycobacterium tuberculosis* DosS

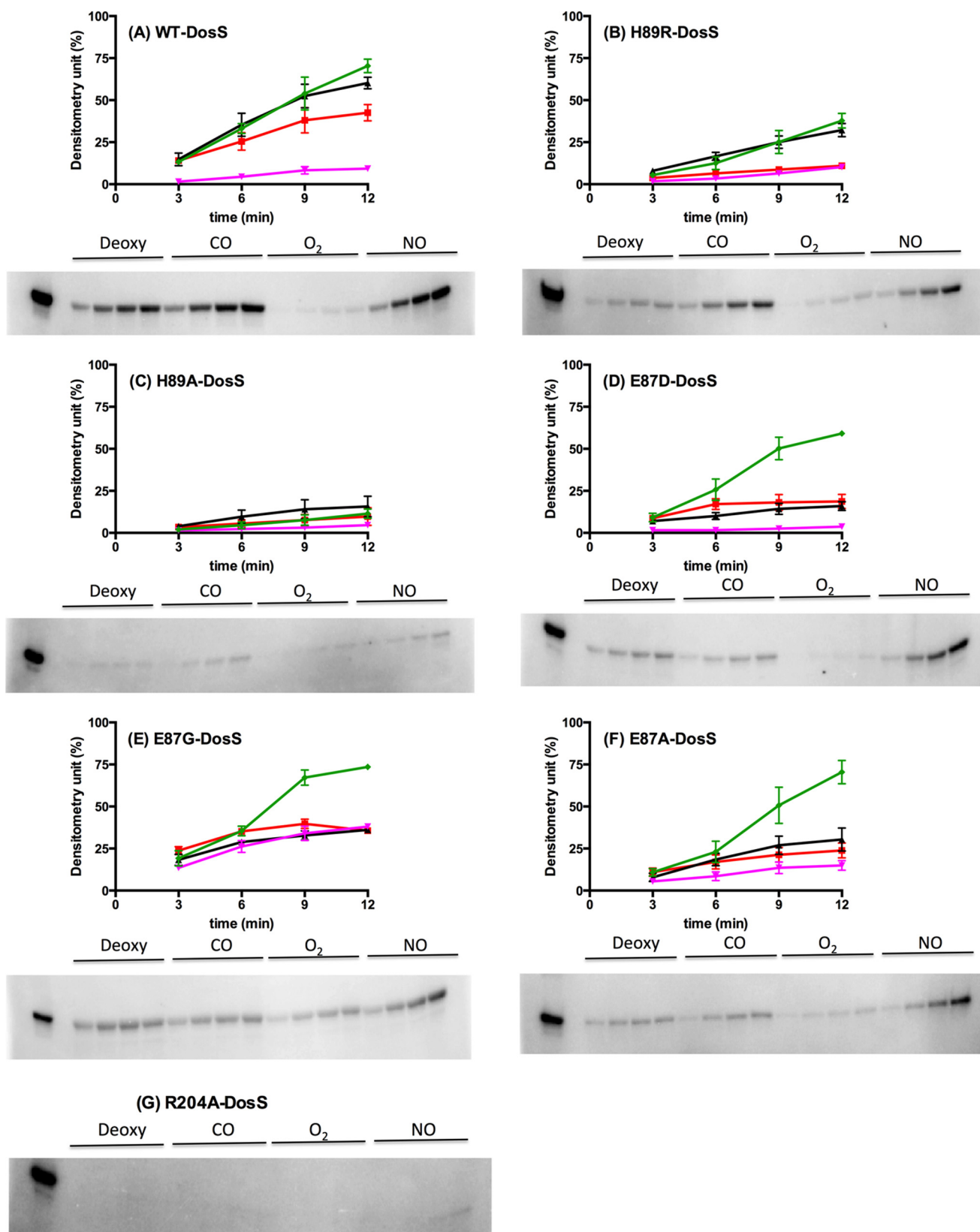


FIGURE 5. Representative autophosphorylation gel and quantification of the activity of wild-type (A), H89R (B), H89A (C), E87D (D), E87G (E), E87A (F), and R204A (G) mutants of DosS in the Fe(II) state (red) and after its exposure to CO (black), O₂ (magenta), and NO (green). 1st lanes, wild-type bound to CO at 20 min; 2nd to 5th lanes, Fe(II); 6th to 9th lanes, exposure of Fe(II) to CO; 10th to 13 lanes, exposure of Fe(II) to O₂; and 13th to 17th lanes, exposure of Fe(II) to NO at 3-, 6-, 9-, and 12-min time points, respectively.

TABLE 1**Quantification of autophosphorylation activity of wild-type DosS and its mutants after 12 min**

The values correspond to the percent conversion relative to a maximum defined by the autophosphorylation observed for the wild-type CO complex after 20 min. Two-way analysis of variance compared with Fe(II).

	Fe(II)	Fe(II)-CO	Fe(II)-O ₂	Fe(II)-NO
WT-DosS	43 ± 8	60 ± 10 ^a	9 ± 3 ^b	70 ± 6 ^b
E87G-DosS	36 ± 3	36 ± 2 (NS) ^c	38 ± 1 (NS)	73 ± 1 ^b
E87A-DosS	23 ± 7	30 ± 12 (NS)	15 ± 5 (NS)	70 ± 12 ^b
E87D-DosS	19 ± 7	16 ± 5 (NS)	4 ± 2 ^d	59 ± 2 ^b
H89R-DosS	11 ± 1	32 ± 8 ^e	10 ± 2 (NS)	38 ± 7 ^b
H89A-DosS	10 ± 10	16 ± 12 (NS)	5 ± 2 (NS)	11 ± 5 (NS)
R204A-DosS	ND ^f	ND	ND	ND

^a $p < 0.01$.

^b $p < 0.0001$.

^c NS mean not significant, $p > 0.05$.

^d $p < 0.05$.

^e $p < 0.001$.

^f ND means not detectable.

modest increase in activity (15%) compared with the wild-type protein (9%), although it was lower than the E87G mutant (38%) (Fig. 5F and Table 1). However, it must be noted that E87G is the only mutant of this position to yield a stable oxy species (Fig. 2D), whereas the others appeared at least partially oxidized. Therefore, the apparent difference in the activities of the oxy states of these mutants may in part reflect oxidation of the E87A and E87D to an essentially inactive ferric state. Overall, the distal glutamic acid mutants recognized and responded to NO as well as the wild-type protein and retained approximately half the activity of the wild type in the Fe(II) deoxy and Fe(II)-CO states.

Arg-204 Mutant—His-89 is in a polar patch of residues within the active site (Fig. 1). It is located close to the junction of the GAF-A and GAF-B domains, so its position in the crystal structure of the isolated GAF-A domain may not accurately reflect its position in the full-length protein. Although not seen in the crystal structures (Fig. 1), molecular dynamics simulations (see below) pointed to a persistent hydrogen bond between His-89 and Arg-204. The interaction between His-89 and Arg-204 was therefore investigated by mutating Arg-204 to Ala, a non-polar residue. The UV-visible spectra of the R204A mutant, which were very similar to those of the other mutants (Fig. 2F), showed normal binding of both CO and NO and autoxidation with O₂. Nevertheless, the autophosphorylation activity of the R204A mutant, both in the absence and presence of ligands, was below the limit of detection for all the forms of the protein (Fig. 5G).

Molecular Dynamics Simulations—Molecular dynamics simulations have been used to investigate the *in vitro* behavior of the wild-type DosS GAF-A domain and its E87A and E87G mutants. Given the complexities and subtleties of inferring structural changes with different gases, we focused these studies on oxygen binding, as this is the situation in which both the E87A and E87G mutants display particularly unusual behavior.

The E87A and E87G mutants had higher activities on exposure to oxygen than the wild-type protein (Table 1). To interpret these results, we considered the impact of active site water molecules on the hydrogen-bonding network depicted in Fig. 1. The wild-type, E87A, and E87G proteins display distinct hydrogen-bonding patterns that are present at varying frequencies throughout the MD simulations. The most frequent possibili-

M. tuberculosis DosS: GLDLEATLRA IVHSATSLVD ARYGAMEVHD RQHRVLHFVY
M. tuberculosis DosT: GLKLDATLRA IVHTAAELVD ARYGALGVRG YDHRVLVEFVY
M. bovis A0A0H3P5J6: GLDLEATLRA IVHSATSLVD ARYGAMEVHD RQHRVLHFVY
M. marinum B2HG12: GLELNATLRT IVHSATNLVD ARYCALLEVHD RDKRVLQFVY
M. ulcerans A0PR05: GLELDATLRT IVHSATNLVD ARYCALLEVHD RDKRVLQFVY

M. tuberculosis DosS: EGIDEETVRR IGHLPKGLGV IGLLIEDPKP LRLDDVS
M. tuberculosis DosT: EGIDEETRHL IGSLPEGRGV LGALIEPKP IRLDDIS
M. bovis A0A0H3P5J6: EGIDEETVRR IGHLPKGLGV IGLLIEDPKP LRLDDVS
M. marinum B2HG12: EGIDEETVRR IGHLPKGLGV IGLLIEDPKP LRLDDIS
M. ulcerans A0PR05: EGIDEETVRR IGHLPKGLGI IGLLIEDPKP LRLDDIS

FIGURE 6. Most frequently observed hydrogen-bonding patterns observed in molecular dynamics simulations for the wild-type DosS GAF-A domain and its E87A and E87G mutants.

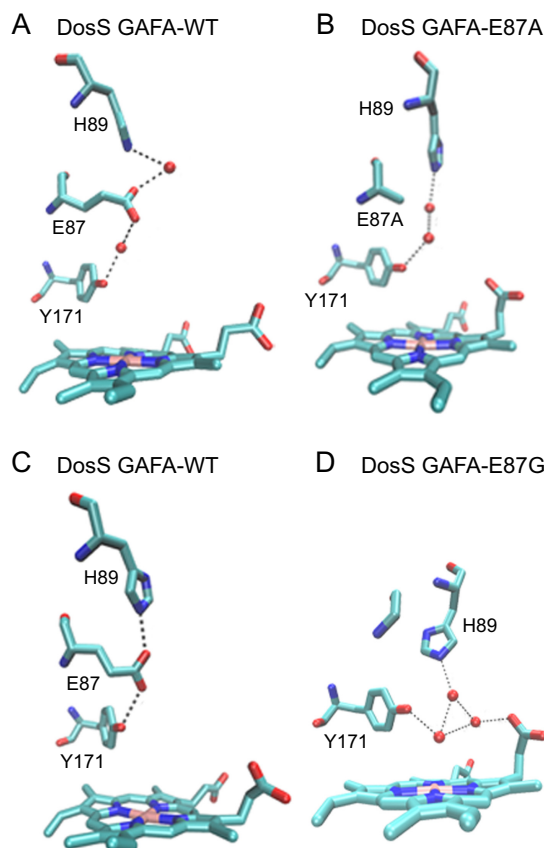


FIGURE 7. Graphic depiction of the hydrogen-bonding patterns observed as a function of time in the molecular dynamics simulations of the wild-type DosS GAF-A (four upper traces) and the E87A mutant (two lower traces). The open circles indicate the presence of the indicated hydrogen-bonding pattern at a given time point in the simulation. The legend on the left indicates the H-bonding pattern.

ties are portrayed in 6. In Fig. 6A, two bridging waters complete the active site hydrogen-bonding network from Tyr-171 to Glu-87 and then to His-89. This is depicted graphically in 7, where open circles indicate the presence of a given bonding network at specific points in the simulation. In the wild-type protein, the Tyr-171–Glu-87 single water bridge (Fig. 7, blue circles in top panel) occurs 49.9% of the time, and the Glu-87–His-89 water bridge (Fig. 7 green circles in top panel) is present in 50.9% of the simulation, although they are both present 33.5% of the time. The wild-type enzyme may also form a network in which there is a direct hydrogen bond between Tyr-171 and Glu-8, and a salt bridge between Glu-87 and His-89 (Fig.

Hydrogen-bonding Network in *Mycobacterium tuberculosis* DosS

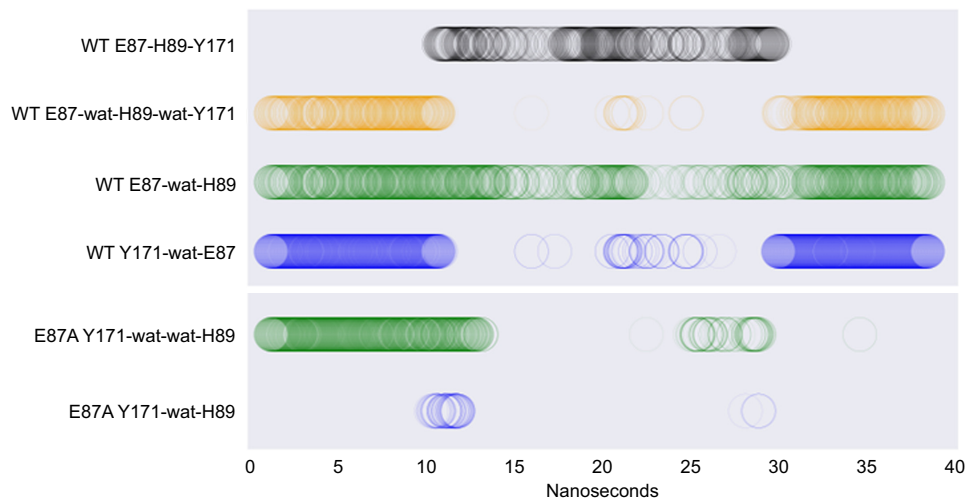


FIGURE 8. Comparison of the local water network in the wild-type ferric enzyme (A) with that of the ferrous enzyme (B). Note the difference in the positions of Glu-87 in the two structures as indicated by the orange discs.

6C). This occurs over 25.5% of the simulation and can be seen graphically as *black circles* in Fig. 7. If we take the overlap of these two cases, the hydrogen-bonding network in the wild-type protein is maintained nearly 60% of the time.

The DosS-E87A mutant does not have the same possibilities for intra-protein hydrogen bonding as the wild type. Because of the non-polar substitution in the E87A mutant, waters are required to bridge the distance from Tyr-171 to His-89. Fig. 6B shows the most common scenario in which two waters bridge the gap. This occurs over 32% of the simulation (Fig. 7, *green circles* in lower panel). It is worth noting that this largely occurs in the first 13 ns of the 40-ns simulation and is almost never revisited. An alternative in which only one hydrogen-bonding water bridges Tyr-171 and His-89 occurs only 1% of the time (Fig. 7, *blue circles* in bottom panel). This probably reflects a low sampling of conformations in which Tyr-171 and His-89 are close enough to be bridged by a single water. It is clear from the last two lines in Fig. 7 that the hydrogen-bonding pattern is severely altered in the E87A mutant. In Fig. 8A the active site water network in the wild-type ferric enzyme is compared with that of the wild-type ferrous enzyme (Protein Data Bank code 2W3F) in which the Glu-87 residue has flipped upwards (Fig. 8B). In the latter case the local water network is obliterated, and this is the environment that oxygen encounters when binding to the Fe(II) enzyme. Consequently, the hydrogen-bonding pattern of the wild-type enzyme may function as a switch that must be disrupted to maintain inactivity on oxygen binding.

Removing the entire Glu-87 side chain, as in the E87G mutant, allows His-89 to penetrate more deeply into the active site, which in turn enables water bridges that can include up to four waters. The most frequent example from the simulations involves an intricate water network, including Tyr-171, three waters, a heme propionate side chain, and His-89 (Fig. 6D).

The effect of global conformational change on the wild-type, E87A, and E87G mutants was analyzed by investigating the root mean squared fluctuation (RMSF) over the course of the simulation. The RMSF of carbon atoms plotted for the E87A (*blue*) and E87G (*orange*) mutants are consistently higher than that of the wild-type (*green*) (Fig. 9A). In particular, the C-terminal

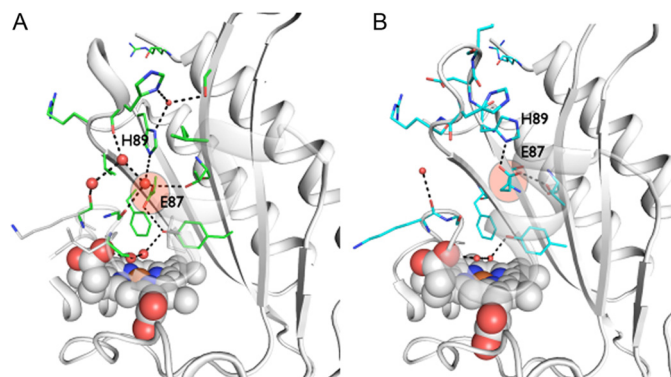


FIGURE 9. A, RMSF plots over the course of the molecular dynamics simulation for the wild-type (*green*), E87A (*blue*), and E87G (*orange*) mutants. To aid in visualizing this fluctuation, an amalgamation of snapshots (every 100 frames) are overlaid in (B and C) for the wild-type and E87A mutants, with each shown in two orientations reflecting a 90° rotation about a vertical axis. The snapshots are color-coded chronologically, with the earliest in *darkest blue* and the latest in *darkest red*. The wild-type has considerably less movement than the E87A mutant.

helix composed of residues 183–204 shows the most consistent RMSF increases in the variants compared with the wild-type protein. This region of the GAF-A domain would be most likely to significantly affect both the positioning of the rest of the DosS protein and interdomain interactions. To aid in visualizing these fluctuations, an amalgamation of snapshots (every 100 frames) are overlaid in Fig. 9 for the wild-type (B) and E87A mutant (C). The wild type has considerably less movement than the E87A (Fig. 9C) mutant, particularly at the interface between the C-terminal helix and residue 204, and the hairpin loop Asp-90–Arg-94. It is possible that this increased fluctuation allows the mutants to continually sample greater conformational space leading to a higher percentage of catalytic events in the absence of CO and NO compared with the wild-type enzyme.

Discussion

DosS is a heme-based sensor that detects changes in intracellular redox state and the presence or absence of gaseous signaling molecules. Understanding the effect of the binding of different gaseous ligands to DosS is important in terms of drug

therapy, as the dormant state of *M. tuberculosis* is less susceptible to the currently available treatment regimens. A crystal structure of the GAF-A domain of wild-type DosS indicated that the carboxyl group of Glu-87 hydrogen-bonds with the hydroxyl of Tyr-171 and the imidazole of His-89, thus forming a hydrogen-bonding network that may be important in the function of the heme center (Fig. 1) (19). In this study, the role of the hydrogen-bonding network in the differential response to gaseous ligands was examined.

It is well established that both DosS and DosT are active as kinases in the Fe(II)-deoxy, Fe(II)-CO, and Fe(II)-NO forms and have little activity in the Fe(III) and Fe(II)-O₂ forms (20, 26). Although DosT forms a stable Fe(II)-O₂ complex, there is disagreement in the literature as to whether DosS is a gas or redox sensor. Parrish *et al.* (2), Ioanoviciu *et al.* (27), and Sousa *et al.* (29) observed stable formation of the Fe(II)-O₂ complex, although other groups have reported immediate oxidation of the Fe(II) to the Fe(III) heme on exposure to O₂ (19, 26, 27). In this study, the UV-visible spectrum of wild-type DosS was recorded in Tris buffer (pH 7.5). Exposure of the Fe(II) wild-type DosS to O₂ resulted in rapid formation of the Fe(III) state, as reported previously (19, 26). However, on pretreating the buffer with Chelex 100, the Fe(II)-O₂ complex was observed with O₂, emphasizing the importance of metal removal for formation of a stable Fe(II)-O₂ complex. All the experiments performed in this study utilized buffers pretreated with Chelex 100. Although not observed by us (27), Cho *et al.* (19) reported that exposure of the ferrous wild-type DosS GAF-A domain to O₂ resulted in its oxidation to the Fe(III) state even when the buffer was chelated. Clearly, autoxidation of the Fe(II)-O₂ state is highly sensitive to the protein and solution environment. The extent to which the mycobacteria respond to the DosS Fe(II)-O₂ complex *versus* the ferric protein is unclear, as both states suppress kinase activity, and we have previously shown that endogenous electron donor proteins can reduce ferric DosS to the ferrous state (27). This ambiguity does not occur with DosT, which gives a highly stable Fe(II)-O₂ complex.

DosT exhibits similar activity to DosS in the presence of gaseous ligands, but it contains Gly and Arg residues at the positions occupied in DosS by Glu-87 and His-89, respectively (Fig. 10). Thus, *a priori*, the E87G and H89R mutants should more closely approximate the environment of DosT in DosS. Furthermore, the DosS E87D mutation should help to preserve the hydrogen-bonding network, whereas the E87A and H89A mutations should disrupt this network. In fact, mutation of Glu-87 to Gly or Ala yielded a protein that formed a stable Fe(II)-O₂ complex or a mixture of the Fe(II)-O₂ and Fe(III) forms, respectively (Fig. 2, D and E), as reported previously (30). Although the E87D mutant also gave rise to a mixture of the Fe(II)-O₂ and Fe(III) forms (Fig. 2C), it exhibited negligible kinase activity (4%) in comparison with the E87G (38%) and E87A (15%) mutants (Table 1). Interestingly, replacement of His-89 by an Ala (H89A) or Arg (H89R) yielded proteins that more readily autoxidized to the ferric state (Fig. 2, A and B), emphasizing the importance of the hydrogen-bonding network in determining the oxidizability of the metal center.

Yukl *et al.* (25) previously demonstrated a critical role for Tyr-171 by establishing that a Y171F mutation disabled kinase

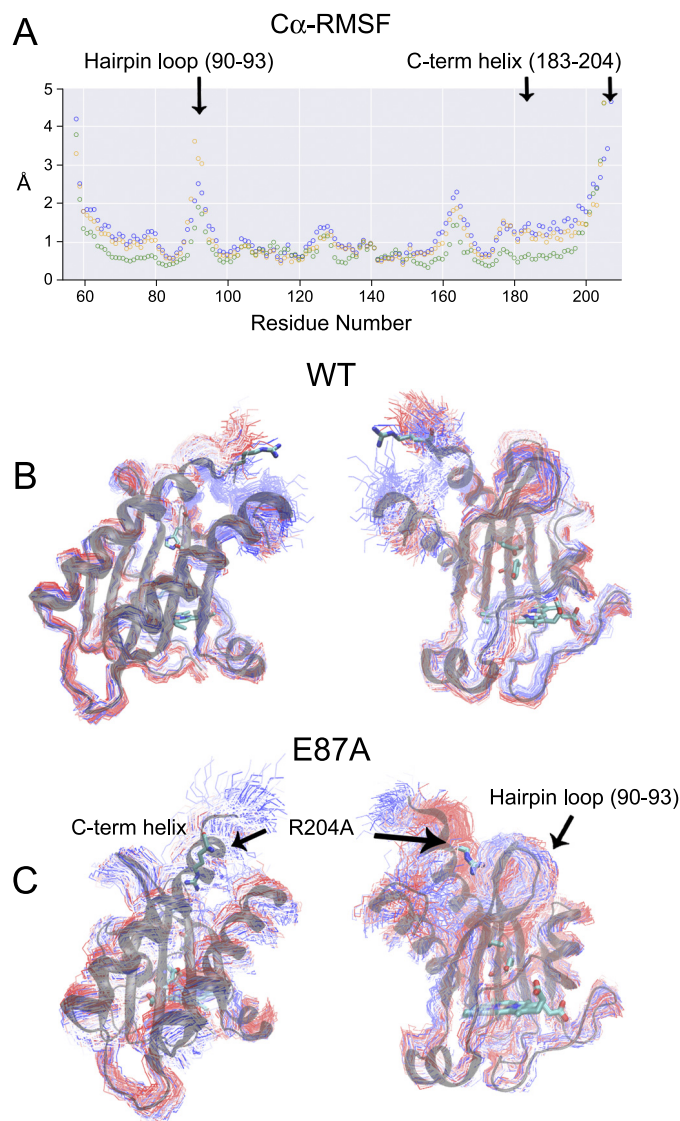


FIGURE 10. Sequence alignment of a region of *M. tuberculosis* DosS and DosT with similar regions from other organisms obtained using Clustal Omega via the web interface, where the sequences are from *M. tuberculosis* DosS, *M. tuberculosis* DosT, *Mycobacterium bovis* A0A0H3P5J6, *Mycobacterium marinum* B2HG12, and *Mycobacterium ulcerans* A0PR05. The numbering indicated at top is from *M. tuberculosis* DosS.

domain autophosphorylation in the presence of all gaseous ligands, while preserving intact the activity of the deoxy state. Tyr-171 is hydrogen-bonded to Glu-87 (Fig. 1). Interestingly, the DosT-like DosS E87G mutant was active in the deoxy form as well as when CO or NO was bound. Most surprisingly, unlike wild-type DosS or DosT, it was also active on binding of O₂. The Fe(II)-O₂ complex of the E87G mutant was red-shifted by 4 nm compared with that of wild-type DosS (Fig. 2D), a difference that may be related to its autophosphorylation activity. Strikingly, both the Y171F and E87G DosS mutants exhibited a loss of ligand discrimination ability, even though their responses were orthogonal to each other. The crystal structure of the E87G GAF-A domain revealed the presence of water molecules at the active site (30). These water molecules, which replace the side chain of the normal Glu residue, can maintain the hydrogen-bonding network from heme to His-89, consistent with our

Hydrogen-bonding Network in *Mycobacterium tuberculosis* DosS

activity assay results. The E87A mutant, which exhibited a decreased activity in all but the Fe(II)-NO state (Fig. 5F), was shown in a previously published crystal structure of the E87A GAF-A domain to have no clear electron density for any water molecules in the active site (30).

The DosS H89R mutant had a kinase activity profile on binding to CO (active), NO (active), and O₂ (low activity) similar to that of wild-type DosS and DosT, even though the activity was reduced (Fig. 5, A and B, and Table 1). The inactivity of the H89R deoxy form may be due to the steric bulk of the Arg residue, which causes Glu-87 to flip to a conformation similar to that in the ferric protein. In contrast, the H89A mutation rendered the protein essentially inactive. Its inactivity suggested that hydrogen-bonding interactions of His-89 play a key role in signal transduction to the kinase domain. Furthermore, molecular dynamics studies indicated that Arg-204 can form a hydrogen bond to His-89 and suggested that mutation of Arg-204 might inactivate the protein. This was confirmed by our finding that the R204A mutant had no measurable kinase activity (Fig. 5G), a finding that provides strong support for the proposed role of this residue.

The results clearly show that the hydrogen-bonding network is important for differential recognition of the gas ligands. We previously showed that Tyr-171 is critical for ligand discrimination, but here we demonstrate that Glu-87 also plays an important role. The E87G and E87A mutants were active as kinases with all the gas ligands, although the E87D mutant had little activity except when NO was bound. The His-89 residue appears to be critical for signal transduction to the kinase domain, as the H89R mutant, which maintained some hydrogen bonding, was partially active, whereas the H89A mutant had no kinase activity above background levels. The disturbance of the distal hydrogen-bonding network in the H89A mutant is also apparent in the resonance Raman data of the H89A CO and NO complexes as they show multiple conformers previously observed with the truncated GAF-A only domain, but not when the GAF-B domain is present. From these data, it is tempting to suggest that GAF-A/GAF-B interdomain interactions play a role in stabilizing the hydrogen-bonding network at the heme distal pocket and the signal transduction to the kinase domain. Finally, the inference from molecular dynamic simulations that Arg-204 hydrogen-bonds to His-89 and that this interaction is important for signal transmission is supported by the finding that mutation of Arg-204 completely inactivates the full-length protein.

Indirect support for a critical role of the hydrogen-bonding network and an interdomain contact involving His-89 and Arg-204 in signal recognition and transmission is provided by the fact that the UV-visible and resonance Raman properties of the wild-type and H89A mutants are essentially identical, which precludes a role for changes in the iron spin state or porphyrin conformation in either these processes.

As shown by the crystal structures of the GAF-A domain of ferric and ferrous DosS (Fig. 8), the catalytically active ferrous protein has a different hydrogen-bonding network than the ferric protein. The partial kinase activity of the ferrous protein, compared with the CO- or NO-bound proteins, is likely to reflect a more mobile active site in the absence of an iron ligand

that allows it to sample both the active and inactive conformations. In the Fe(II)-O₂ complex the terminal oxygen of the dioxygen ligand is a good hydrogen-bond acceptor and, like the water ligand of the ferric state, supports a hydrogen bond network that stabilizes the catalytically inactive state. In contrast, in the Fe(II)-CO and Fe(II)-NO complexes, the poorer hydrogen bonding properties of the terminal oxygen of the CO and NO give rise to hydrogen-bonding patterns that more closely resemble that of the ferrous, ligand-free, catalytically active protein. In this conformation, Glu-87 swings upward (Fig. 8), and this shift of Glu-87 may be important for activation of the kinase domain.

Author Contributions—D. B. did all the analytical work on DosS and its mutants; Y. M. did the molecular dynamics simulations; E. T. Y. carried out resonance Raman spectroscopy; S. S. designed and verified the plasmids, and C. R. N. expressed the E87A DosS mutant. P. M. L. directed and funded the resonance Raman work, and P. R. O. M. conceived, funded, and directed the project. All the authors participated in writing the manuscript.

Acknowledgments—We thank Relly Brandman for preliminary molecular dynamics studies and Nancy Phillips for improving the figures.

References

1. Dye, C., Scheele, S., Dolin, P., Pathania, V., and Ravigliione, M. C. (1999) Consensus statement. Global burden of tuberculosis: estimated incidence, prevalence, and mortality by country. WHO Global Surveillance and Monitoring Project. *J. Am. Med. Assoc.* **282**, 677–686
2. Parrish, N. M., Dick, J. D., and Bishai, W. R. (1998) Mechanisms of latency in *Mycobacterium tuberculosis*. *Trends Microbiol.* **6**, 107–112
3. Fenton, M. J., Vermeulen, M. W., Kim, S., Burdick, M., Strieter, R. M., and Kornfeld, H. (1997) Induction of γ interferon production in human alveolar macrophages by *Mycobacterium tuberculosis*. *Infect. Immun.* **65**, 5149–5156
4. Silva-Gomes, S., Appelberg, R., Larsen, R., Soares, M. P., and Gomes, M. S. (2013) Heme catabolism by heme oxygenase-1 confers host resistance to *Mycobacterium* infection. *Infect. Immun.* **81**, 2536–2545
5. Regev, D., Surolia, R., Karki, S., Zolak, J., Montes-Worboys, A., Oliva, O., Guroji, P., Saini, V., Steyn, A. J., Agarwal, A., and Antony, V. B. (2012) Heme oxygenase-1 promotes granuloma development and protects against dissemination of mycobacteria. *Lab. Invest.* **92**, 1541–1552
6. Dick, T. (2001) Dormant tubercle bacilli: the key to more effective TB chemotherapy? *J. Antimicrob. Chemother.* **47**, 117–118
7. Wayne, L. G. (2001) *In vitro* model of hypoxically induced nonreplicating persistence of *Mycobacterium tuberculosis*. *Methods Mol. Med.* **54**, 247–269
8. Wayne, L. G., and Sohaskey, C. D. (2001) Nonreplicating persistence of *Mycobacterium tuberculosis*. *Annu. Rev. Microbiol.* **55**, 139–163
9. Voskuil, M. I., Schnappinger, D., Visconti, K. C., Harrell, M. I., Dolganov, G. M., Sherman, D. R., and Schoolnik, G. K. (2003) Inhibition of respiration by nitric oxide induces a *Mycobacterium tuberculosis* dormancy program. *J. Exp. Med.* **198**, 705–713
10. Betts, J. C., Lukey, P. T., Robb, L. C., McAdam, R. A., and Duncan, K. (2002) Evaluation of a nutrient starvation model of *Mycobacterium tuberculosis* persistence by gene and protein expression profiling. *Mol. Microbiol.* **43**, 717–731
11. Schnappinger, D., Ehrt, S., Voskuil, M. I., Liu, Y., Mangan, J. A., Monahan, I. M., Dolganov, G., Efron, B., Butcher, P. D., Nathan, C., and Schoolnik, G. K. (2003) Transcriptional adaptation of *Mycobacterium tuberculosis* within macrophages: insights into the phagosomal environment. *J. Exp. Med.* **198**, 693–704

12. Sharma, S. K., and Mohan, A. (2006) Multidrug-resistant tuberculosis. A menace that threatens to destabilize tuberculosis control. *Chest* **130**, 261–272
13. Roberts, D. M., Liao, R. P., Wisedchaisri, G., Hol, W. G., and Sherman, D. R. (2004) Two sensor kinases contribute to the hypoxic response of *Mycobacterium tuberculosis*. *J. Biol. Chem.* **279**, 23082–23087
14. Honaker, R. W., Dhiman, R. K., Narayanasamy, P., Crick, D. C., and Voskuil, M. I. (2010) DosS responds to a reduced electron transport system to induce the *Mycobacterium tuberculosis* DosR regulon. *J. Bacteriol.* **192**, 6447–6455
15. Dasgupta, N., Kapur, V., Singh, K. K., Das, T. K., Sachdeva, S., Jyothisri, K., and Tyagi, J. S. (2000) Characterization of a two-component system, devR-devS, of *Mycobacterium tuberculosis*. *Tuber. Lung Dis.* **80**, 141–159
16. Gautam, U. S., McGillivray, A., Mehra, S., Didier, P. J., Midkiff, C. C., Kisse, R. S., Golden, N. A., Alvarez, X., Niu, T., Rengarajan, J., Sherman, D. R., and Kaushal, D. (2015) DosS is required for the complete virulence of *Mycobacterium tuberculosis* in mice with classical granulomatous lesions. *Am. J. Respir. Cell Mol. Biol.* **52**, 708–716
17. Kumar, A., Deshane, J. S., Crossman, D. K., Bolisetty, S., Yan, B. S., Kramnik, I., Agarwal, A., and Steyn, A. J. (2008) Heme oxygenase-1-derived carbon monoxide induces the *Mycobacterium tuberculosis* dormancy regulon. *J. Biol. Chem.* **283**, 18032–18039
18. Sardiwal, S., Kendall, S. L., Movahedzadeh, F., Rison, S. C., Stoker, N. G., and Djordjevic, S. (2005) A GAF domain in the hypoxia/NO-inducible *Mycobacterium tuberculosis* DosS protein binds haem. *J. Mol. Biol.* **353**, 929–936
19. Cho, H. Y., Cho, H. J., Kim, Y. M., Oh, J. I., and Kang, B. S. (2009) Structural insight into the heme-based redox sensing by DosS from *Mycobacterium tuberculosis*. *J. Biol. Chem.* **284**, 13057–13067
20. Ioanoviciu, A., Yukl, E. T., Moënne-Loccoz, P., and de Montellano, P. R. (2007) DevS, a heme-containing two-component oxygen sensor of *Mycobacterium tuberculosis*. *Biochemistry* **46**, 4250–4260
21. Podust, L. M., Ioanoviciu, A., and Ortiz de Montellano, P. R. (2008) 2.3 Å x-ray structure of the heme-bound GAF domain of sensory histidine kinase DosT of *Mycobacterium tuberculosis*. *Biochemistry* **47**, 12523–12531
22. Humphrey, W., Dalke, A., and Schulten, K. (1996) VMD: visual molecular dynamics. *J. Mol. Graph.* **14**, 33–38
23. Best, R. B., Zhu, X., Shim, J., Lopes, P. E., Mittal, J., Feig, M., and Mackerell, A. D., Jr. (2012) Optimization of the additive CHARMM all-atom protein force field targeting improved sampling of the backbone φ , ψ and side-chain $\chi(1)$ and $\chi(2)$ dihedral angles. *J. Chem. Theory Comput.* **8**, 3257–3273
24. Phillips, J. C., Braun, R., Wang, W., Gumbart, J., Tajkhorshid, E., Villa, E., Chipot, C., Skeel, R. D., Kalé, L., and Schulten, K. (2005) Scalable molecular dynamics with NAMD. *J. Comput. Chem.* **26**, 1781–1802
25. Yukl, E. T., Ioanoviciu, A., Nakano, M. M., de Montellano, P. R., and Moënne-Loccoz, P. (2008) A distal tyrosine residue is required for ligand discrimination in DevS from *Mycobacterium tuberculosis*. *Biochemistry* **47**, 12532–12539
26. Kumar, A., Toledo, J. C., Patel, R. P., Lancaster, J. R., Jr., and Steyn, A. J. (2007) *Mycobacterium tuberculosis* DosS is a redox sensor and DosT is a hypoxia sensor. *Proc. Natl. Acad. Sci. U.S.A.* **104**, 11568–11573
27. Ioanoviciu, A., Meharena, Y. T., Poulos, T. L., and Ortiz de Montellano, P. R. (2009) DevS oxy complex stability identifies this heme protein as a gas sensor in *Mycobacterium tuberculosis* dormancy. *Biochemistry* **48**, 5839–5848
28. Yukl, E. T., Ioanoviciu, A., de Montellano, P. R., and Moënne-Loccoz, P. (2007) Interdomain interactions within the two-component heme-based sensor DevS from *Mycobacterium tuberculosis*. *Biochemistry* **46**, 9728–9736
29. Sousa, E. H., Tuckerman, J. R., Gonzalez, G., and Gilles-Gonzalez, M. A. (2007) DosT and DevS are oxygen-switched kinases in *Mycobacterium tuberculosis*. *Protein Sci.* **16**, 1708–1719
30. Cho, H. Y., Cho, H. J., Kim, M. H., and Kang, B. S. (2011) Blockage of the channel to heme by the E87 side chain in the GAF domain of *Mycobacterium tuberculosis* DosS confers the unique sensitivity of DosS to oxygen. *FEBS Lett.* **585**, 1873–1878